Dalton Transactions

An international journal of inorganic chemistry

www.rsc.org/dalton

Number 36 | 28 September 2007 | Pages 3973–4104

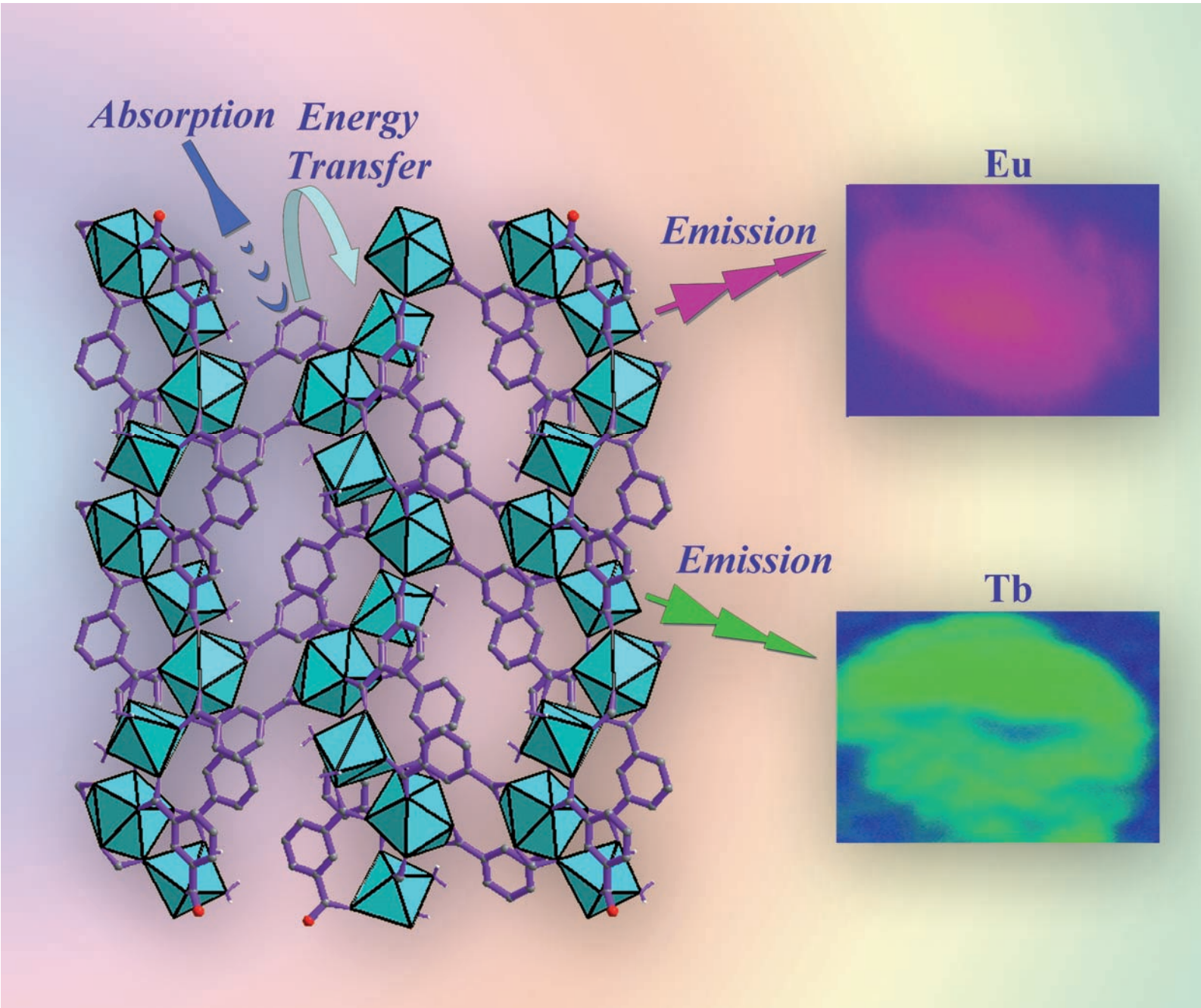

ISSN 1477-9226

PAPER
Partha Mahata, K. V. Ramya and Srinivasan Natarajan
Synthesis, structure and optical properties of rare-earth benzene carboxylates

PERSPECTIVE
Trevor W. Hambley *et al.*
Bioreductive activation and drug chaperoning in cobalt pharmaceuticals

RSC Publishing

1477-9226(2007)36;1-1

Synthesis, structure and optical properties of rare-earth benzene carboxylates†‡

Partha Mahata, K. V. Ramya and Srinivasan Natarajan*

Received 26th April 2007, Accepted 25th June 2007
First published as an Advance Article on the web 13th July 2007
DOI: 10.1039/b706363f

Two series of rare-earth isophthalates of the general formula, $[M_2(H_2O)][\{C_6H_4(COO)_2\}_2\text{-}\{C_6H_4(COOH)(COO)\}_2]\cdot H_2O$, M = La (**I**), Pr (**Ia**), and Nd (**Ib**) and $[M_2(H_2O)_2]\text{-}[\{C_6H_4(COO)_2\}_3]\cdot H_2O$, M = Y (**II**), Gd (**IIa**), and Dy (**IIb**) have been prepared by the reaction of the corresponding trivalent lanthanide salts and isophthalic acid under mild hydrothermal conditions. The La (**I**), Pr (**Ia**) and Nd (**Ib**) have MO_9 polyhedra connected to the isophthalate anions forming a two-dimensional structure, whereas Y (**II**), Gd (**IIa**) and Dy (**IIb**) have MO_7 and MO_8 polyhedral units connected to the isophthalate anions forming a different, but related two-dimensional structure. Both the structures are stabilized by hydrogen bonding and $\pi\cdots\pi/CH\cdots\pi$ interactions. Partial substitution of Eu and Tb (2 and 4%) at the La (**I**) and Y (**II**) sites give rise to characteristic red/pink or green luminescence, indicating a ligand-sensitized metal-centered emission. The Nd (**Ib**) compound shows interesting UV and blue emission through an up-conversion process.

Introduction

Research on rare-earth based compounds has attracted increasing attention due to their interesting luminescence properties. Lanthanide compounds exhibit intense luminescence and are useful in biochemical fluorescent probes in addition to other emission based applications.[1] In all the compounds, the f electron remains highly localized and the emission behavior of the rare-earth ions, based on the f–f transitions, have narrow wavelength ranges and high quantum yields, which makes them attractive for light emitting device (LED) applications. The f–f transitions are spin and parity forbidden, and to exploit the luminescent properties, ligands that function as sensitizers are employed. Recent studies show that benzoic acid and its derivatives offer an excellent choice to sensitize and observe the lanthanide emission. Among the lanthanide ions, Eu^{3+} and Nd^{3+} are two of the most important elements to use as optical centers. Eu^{3+} compounds are attractive for use in the visible region ($\lambda = 615$ nm), while Nd^{3+} compounds are useful in the near IR region ($\lambda = 800$–1700 nm). In addition, Nd^{3+} compounds also show up-conversion behavior of converting the IR radiation into visible region, *via* a two photon absorption process.[2]

In spite of the vast advances made in the understanding of the optical properties of the rare-earth ions, the subtle relationship that exists between the photophysical behavior and the structure points towards the need to explore many new structures for fruitfully exploiting the emission property of the rare-earth ions.[3] In light of this, the recently discovered rare-earth benzene carboxylates are good candidates to investigate both the structure as well as the luminescent properties.[4] The design and synthesis of lanthanide benzene carboxylates, however, appears to be a difficult task primarily due to the higher and varied coordination requirements of the lanthanide ions.[5]

We have been interested in the study of aromatic (benzene, pyridine) dicarboxylate compounds of lanthanide and related systems, resulting in a large number of new and novel structures.[6] In the present study, we have used isophthalic acid along with the lanthanide ions. Isophthalic acid has been widely used for the preparation of metal–organic framework compounds of lanthanides.[7] During the course our investigations, we have prepared new two-dimensional lanthanide isophthalates $[M_2(H_2O)][\{C_6H_4(COO)_2\}_2\{C_6H_4(COOH)(COO)\}_2]\cdot H_2O$, M = La (**I**), Pr (**Ia**) and Nd (**Ib**) and $[M_2(H_2O)_2][\{C_6H_4(COO)_2\}_3]\cdot H_2O$, M = Y (**II**), Gd (**IIa**) and Dy (**IIb**). Of these, compounds with La (**I**), Y (**II**) and Gd (**IIa**) have been obtained as good quality single crystals, while the Pr (**Ia**), Nd (**Ib**) and Dy (**IIb**) are formed as pure powder samples. The La (**I**), Pr (**Ia**) and Nd (**Ib**) have MO_9 polyhedra connected to the isophthalate anion forming two-dimensional structures, whereas Y (**II**), Gd (**IIa**) and Dy (**IIb**) have MO_7 and MO_8 polyhedral units connected with the isophthalate anions forming a related two-dimensional structure. Doping of 2% and 4% Eu^{3+} or Tb^{3+} in place of La^{3+} (**I**) and Y^{3+} (**II**) clearly show metal-centered emission. The Nd (**Ib**) compound show interesting UV and blue emission through a two-photon up-conversion process. In this paper, we report the synthesis, structure and photophysical properties of these compounds.

Experimental

Synthesis and initial characterization

All the compounds were prepared employing the hydrothermal method. In a typical synthesis, for **I**, La_2O_3 (0.082 g, 0.5 mM) was dispersed in 3 mL of water. To this, isophthalic acid (0.168 g,

Framework Solids Laboratory, Solid State and Structural Chemistry Unit, Indian Institute of Science, Bangalore, 560 012, India. E-mail: snatarajan@sscu.iisc.ernet.in

† CCDC reference numbers 641732–641734. For crystallographic data in CIF or other electronic format see DOI: 10.1039/b706363f

‡ Electronic supplementary information (ESI) available: Powder X-ray diffraction patterns; TGA studies; IR, UV-Vis and photoluminescence spectra; coordination modes of the isophthalate anions and additional figures; and selected bond angles for **I**, **II** and **IIa**. See DOI: 10.1039/b706363f

1 mM), pyridine-2,6-dicarboxylic acid (0.17 g, 1 mM) and NaOH (0.08 g, 2 mM) were added under continuous stirring. The mixture was homogenized for 30 min at room temperature. The final mixture was then sealed in a 7 mL PTEF lined autoclave and heated at 150 °C for 5 days and 180 °C for 2 days under autogeneous pressure. The initial pH of the reaction mixture was 3, and no appreciable change in pH was noted after the reaction. The final product, containing large quantities of colorless block type crystals, was filtered, washed with deionized water under vacuum, and dried at ambient conditions (yield ~70% based on La). For the preparation of isostructural Pr (**Ia**) and Nd (**Ib**) compounds, Pr_2O_3 (0.083 g, 0.5 mM) and Nd_2O_3 (0.085 g, 0.5 mM) were used in place of La_2O_3 by keeping the composition and the reaction conditions identical to those in **I**. In both cases, the resulting product contained large quantities of pale green (Pr) and pale violet (Nd) powder with similar yields. For **II** and **IIa**, $Y(NO_3)_3$ and $Gd(NO_3)_3$ (0.0916 g of $Y(NO_3)_3$, 0.1144 g of $Gd(NO_3)_3$, 0.33 mM) was dissolved in 4 mL of Millipore water. To this, isophthalic acid (0.056 g, 0.33 mM), pyridine-2,3-dicarboxylic acid (0.056, 0.33 mM) and NaOH (0.027 g, 0.67 mM) were added under continuous stirring. The mixture was homogenized for 30 min at room temperature. The final mixture was sealed in a 7 mL PTEF lined autoclave and heated at 180 °C for 3 days under autogeneous pressure. In both cases, the resulting product contained large quantities of colorless block type crystals with high yields (~ 70%). For the preparation of isostructural Dy compound (**IIb**), $Dy(NO_3)_3$ (0.1161 g, 0.33 mM) was used in place of Y. The resulting product contained large quantities of white powder with similar yields. The Eu (2 mol%, **Ic**, 4 mol%, **Id**) and Tb (2 mol%, **Ie**, 4 mol%, **If**) substituted compounds in place of La (**I**) and Eu (2 mol%, **IIc**, 4 mol%, **IId**) and Tb (2 mol%, **IIe**, 4 mol%, **IIf**) substituted compounds in place of Y (**II**) were prepared employing similar synthetic procedures resulting in a fine uniform powder samples with high yields. Though a secondary acid, pyridine-2,6-dicarboxylic acid for **I** and pyridine-2,3-dicarboxylic acid for **II**, has been employed during the synthesis, the final product contained only isophthalic acid. The exact role of the secondary acid is still not clear. It is likely that the role is to control the pH of the reaction mixture. We have not been able to prepare the present compounds in the absence of a secondary acid in the reaction mixture. Anal. Calcd for **I**: C 39.48, H 2.26. Found: C 39.21, H 2.17%. Anal. Calcd for **Ia**: C 39.33, H 2.25. Found: C 39.09, H 2.18%. Anal. Calcd for **Ib**: C 39.06, H 2.24. Found: C 39.2, H 2.11%. Anal. Calcd for **Ic**: C 39.49, H 2.26. Found: C 39.26, H 2.09%. Anal. Calcd for **Id**: C 39.47, H 2.26. Found: C 39.19, H 2.15%. Anal. Calcd for **Ie**: C 39.48, H 2.26. Found: C 39.15, H 2.12%. Anal. Calcd for **If**: C 39.45, H 2.26. Found: C 39.25, H 2.14%. Anal. Calcd for **II**: C 39.88, H 2.22. Found: C 39.35, H 2.09%. Anal. Calcd for **IIa**: C 33.53, H 1.86. Found: C 32.96, H 1.69%. Anal. Calcd for **IIb**: C 33.13, H 1.84. Found: C 33.02, H 1.63%. Anal. Calcd for **IIc**: C 39.76, H 2.20. Found: C 39.49, H 2.11%. Anal. Calcd for **IId**: C 39.62, H 2.20. Found: C 39.37, H 2.06%. Anal. Calcd for **IIe**: C 39.74, H 2.20. Found: C 39.45, H 2.13%. Anal. Calcd for **IIf**: C 39.59, H 2.20. Found: C 39.29, H 2.08%.

Powder X-ray diffraction (XRD) patterns were recorded on crushed single crystals in the 2θ range 5–50° using Cu Kα radiation (Philips X'part) (see ESI‡). The XRD patterns indicated that the products were new materials; the patterns being entirely consistent with the simulated XRD pattern generated based on the structures determined using the single-crystal XRD. Thermogravimetric analysis (TGA) has been carried out in air (flow rate = 20 mL min^{-1}) in the temperature range 30–850 °C (heating rate = 5 °C min^{-1}) (see ESI‡). The TGA studies indicate that the compounds with the structure of **I** (La, Pr, Nd) behave differently compared to the compounds of **II** (Y, Gd and Dy). For the compounds of **I**, we observed weight loss at 100, 190, 300 and 540 °C. For compounds of **II**, there were three weight losses at 100, 280 and 570 °C. In both cases, the observed loss at each step could not be correlated clearly with the structure and the decomposition behavior appears to be complicated. The total observed weight loss of both series (**I** and **II**) corresponds well with the loss of the carboxylate and the water molecules 69% (calc. 66.5%), 66% (calc. 65.13%), 63.8% (calc. 65.78%), 72% (calc. 68.74%), 59.5% (calc. 57.8%), and 57.2% (calc. 57.1%) for **I**, **Ia**, **Ib**, **II**, **IIa**, and **IIb**, respectively. The final calcined product was found to be crystalline by powder XRD and corresponds to La_2O_3 (JCPDS No. 74–1144), Pr_6O_{11} (JCPDS No. 42–1121), Nd_2O_3 (JCPDS No. 83–1346), Y_2O_3 (JCPDS No. 86–1326), Gd_2O_3 (JCPDS No. 74–1987), and Dy_2O_3 (JCPDS No. 86–1327), respectively. IR spectra were recorded as KBr pellet (Perkin Elmer, SPECTRUM 1000). The observed IR bands are listed in Table 1. We have also observed a band at ~1690 cm^{-1} characteristic of C–OH in the case of the compounds with structure **I**.[8]

Single crystal structure determination

A suitable single crystal of each compound was carefully selected under a polarizing microscope and glued to a thin glass fiber. The single crystal data were collected on a Bruker AXS smart

Table 1 The observed IR bands for $M_2(H_2O)][\{C_6H_4(COO)_2\}_2\{C_6H_4(COOH)(COO)\}_2]\cdot H_2O$, M = La (**I**), M = Pr (**Ia**) and (c) M = Nd (**Ib**) and $[M_2(H_2O)_2][\{C_6H_4(COO)_2\}_3]\cdot H_2O$, M = Y (**II**), M = Gd (**IIa**) and (c) M = Dy (**IIb**)

Bands	**I**/cm^{-1}	**Ia**/cm^{-1}	**Ib**/cm^{-1}	**II**/cm^{-1}	**IIa**/cm^{-1}	**IIb**/cm^{-1}
ν_{as}(O–H)	3252 (s)	3218(s)	3207 (s)	3263 (s)	3316 (s)	3276 (s)
ν_s(C–H)$_{aromatic}$	3062 (w)	3051 (w)	3073 (s)	3079 (w)	3079 (w)	3079 (w)
ν_s(C–OH)	1690 (m)	1690 (m)	1690 (m)	Absent	Absent	Absent
ν_s(C=O)	1615 (s)	1612 (s)	1612 (s)	1609 (s)	1622 (s)	1618 (s)
$\delta(H_2O)$	1550 (s)	1552 (s)	1550 (s)	1543 (s)	1540 (s)	1530 (s)
δ(COO)	1408 (s)	1408 (s)	1408 (s)	1398 (s)	1395 (s)	1396 (s)
δ(CH$_{aromatic}$)$_{in\text{-}of\text{-}plane}$	1155 (m)	1168 (m)	1160 (m)	1175 (w)	1167 (w)	1162 (w)
ν_s(C–C)$_{skeletal}$	945 (m)	956 (m)	950 (m)	939 (w)	942 (w)	939 (w)
δ(CH$_{aromatic}$)$_{out\text{-}of\text{-}plane}$	840 (s)	842 (s)	837 (s)	830 (m)	821 (m)	825 (m)

Apex CCD diffractometer at 293(2) K. The X-ray generator was operated at 50 kV and 35 mA using Mo Kα (λ = 0.71073 Å) radiation. Data were collected with ω scan width of 0.3°. A total of 606 frames were collected in three different setting of ϕ (0, 90, 180°) keeping the sample-to-detector distance fixed at 6.03 cm and the detector position (2θ) fixed at −25°. The data were reduced using SAINTPLUS,[9] and an empirical absorption correction was applied using the SADABS program.[10] The structure was solved and refined using SHELXL97[11] present in the WinGx suit of programs (Version 1.63.04a).[12] All the hydrogen atoms of the carboxylic acids, and the bound as well as the lattice water molecules, were initially located in the difference Fourier maps, and for the final refinement, the hydrogen atoms were placed in geometrically ideal positions and refined in the riding mode. In all three compounds restraints for the bond distances were used during the refinement for keeping the hydrogen atoms bonded with the water molecules. Final refinement included atomic positions for all the atoms, anisotropic thermal parameters for all the non-hydrogen atoms, and isotropic thermal parameters for all the hydrogen atoms. Full-matrix least-squares refinement against $|F^2|$ was carried out using the WinGx package of programs.[12] Details of the structure solution and final refinements for **I**, **II** and **Ia** are given in Table 2.

Results and discussion

Structure

The compound **I** has 52 non-hydrogen atoms in the asymmetric unit, of which two La^{3+} ions are crystallographically independent. The isophthalate anions can be classified into four crystallographically distinct based on their coordination modes (see ESI‡). Both the La^{3+} ions have nine coordination with oxygens (La(1) = 8 carboxylate oxygens and a water molecule and La(2) = 9 carboxylate oxygens) that form a distorted tricapped trigonal prismatic arrangement around the central La^{3+} ion (see ESI‡). Of the 18 oxygens in the asymmetric unit, five oxygens [O(2), O(3), O(4), O(5) and O(8)] have μ_3 connectivity linking two lanthanide centers and a carbon atom. The presence of μ_3 oxygens in **I** gives rise to infinite La–O–La one-dimensional connectivity. The La–O bonds have distances in the range 2.361(2)–2.745(2) and the O–La–O bond angles are in the range 48.78(6)–159.18(7)°. We arrive at the coordination geometry around the La^{3+} ions based on the typical bond distances in the range 2.2–2.8 Å. Similar bond distances and angles have been observed before.[4c] Selected bond distances for **I** are listed in Table 3.

The two-dimensional structure of **I** can be easily understood by considering the connectivity between the La^{3+} ions. Thus, La(1) and La(2) ions are connected through three μ_3 oxygens [O(2), O(3) and O(4)] to form a face-shared dimer. The dimer units are connected edge-wise through two μ_3 oxygens [O(5) and O(8)] giving rise to an infinite one-dimensional La–O–La chains (Fig. 1a). The M–M distances in **I** have two distinct values, one corresponding to the face-shared dimer (3.973 Å) and the other due to the sharing of the edges (4.120 Å). One isophthalate anion

Table 3 Selected bond distances (Å) observed in $[La_2(H_2O)][\{C_6H_4(COO)_2\}_2\{C_6H_4(COOH)(COO)\}_2]\cdot H_2O$, **I**

Bond	Amplitude	Bond	Amplitude
La(1)–O(1)	2.659(2)	La(2)–O(2)	2.523(2)
La(1)–O(2)	2.651(2)	La(2)–O(3)	2.737(2)
La(1)–O(3)	2.553(2)	La(2)–O(4)	2.615(2)
La(1)–O(4)	2.471(2)	La(2)–O(5)[a]	2.700(2)
La(1)–O(5)	2.580(2)	La(2)–O(8)[a]	2.490(2)
La(1)–O(6)	2.446(2)	La(2)–O(10)	2.491(2)
La(1)–O(7)	2.558(3)	La(2)–O(11)	2.605(2)
La(1)–O(8)	2.745(2)	La(2)–O(12)	2.535(2)
La(1)–O(9)	2.472(2)	La(2)–O(13)	2.361(2)

[a] Symmetry transformations used to generate equivalent atoms: $-x$, $y + 1/2$, $-z + 1/2$.

Table 2 Crystal data and structure refinement parameters for $[La_2(H_2O)][\{C_6H_4(COO)_2\}_2\{C_6H_4(COOH)(COO)\}_2]\cdot H_2O$, **I**, $[M_2(H_2O)_2][\{C_6H_4(COO)_2\}_3]\cdot H_2O$, M = Y (**II**), Gd (**IIa**)

Structure parameter	**I**	**II**	**IIa**
Empirical formula	$C_{32}H_{22}La_2O_{18}$	$C_{24}H_{16}O_{15}Y_2$	$C_{24}H_{16}O_{15}Gd_2$
Formula weight	972.32	722.19	858.87
Crystal system	Monoclinic	Monoclinic	Monoclinic
Space group	$P2_1/c$ (no.14)	$P2_1/c$ (no.14)	$P2_1/c$ (no.14)
a/Å	10.3780(19)	10.587(2)	10.6293(18)
b/Å	14.177(3)	14.227(3)	14.219(2)
c/Å	21.525(4)	17.130(3)	17.175(3)
α/°	90.0	90.0	90.0
β/°	95.710(3)	97.998(4)	97.915
γ/°	90.0	90.0	90.0
Volume/Å^3	3151.3(10)	2554.8(8)	2571.2(8)
Z	4	4	4
T/K	293(2)	293(2)	293(2)
ρ_{calc}/g cm^{-3}	2.049	1.878	2.219
μ/mm^{-1}	2.763	4.599	5.192
θ range/°	1.72 to 28.00	1.87 to 28.01	1.87 to 28.03
λ (Mo Kα)/Å	0.71073	0.71073	0.71073
R indices [$I > 2\sigma(I)$]	$R_1 = 0.0309$, w$R_2 = 0.0559$	$R_1 = 0.0529$, w$R_2 = 0.0896$	$R_1 = 0.0297$, w$R_2 = 0.0537$
R indices (all data)	$R_1 = 0.0430$, w$R_2 = 0.0591$	$R_1 = 0.1083$, w$R_2 = 0.1054$	$R_1 = 0.0387$, w$R_2 = 0.0563$

$R_1 = \Sigma \, \| F_0 | - | F_c | / \Sigma \, | F_0 |$; w$R_2 = \{\Sigma[w(F_0^2 - F_c^2)^2]/\Sigma[w(F_0^2)^2]\}^{1/2}$. $w = 1/[\sigma^2(F_0)^2 + (aP)^2 + bP]$, $P = [\max.(F_0^2,0) + 2(F_c)^2]/3$, where $a = 0.0229$ and $b = 0$ for **I**, $a = 0.0415$ and $b = 0$ for **II** and $a = 0.0189$ and $b = 2.0973$ for **IIa**.

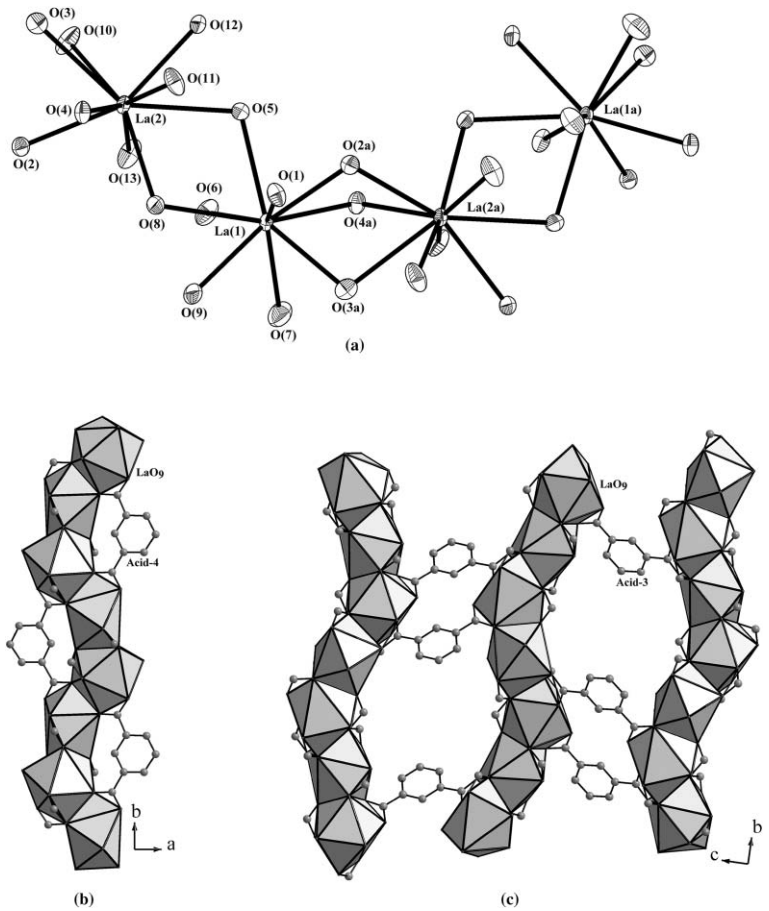

Fig. 1 (a) ORTEP[22] diagram showing the connectivity between La(1)O_9 and La(2)O_9 polyehedra by the μ_3 oxygen atoms. Thermal ellipsoids are given at 50% probability. Note the formation of the face-shared dimers (see text). Symmetry transformations used to generate equivalent atoms: La(1a) $-x$, $1/2 + y$, $1/2 - z$ and La(2a) $-x$, $-1/2 + y$, $1/2 - z$, O(2a, 3a or 4a) $-x$, $-1/2 + y$, $1/2 - z$. (b) Figure showing the one-dimensional La–O–La chains. Note that acid-4 links within the chain. (c) View of two-dimensional layer formed by the connectivity between two La–O–La chains and acid-3.

(acid-4) connect the La^{3+} ions within the chain, as shown in Fig. 1b. The isophthalate anions (acid-1 and acid-2), which are monoionic, connects with this chain through only one end of the carboxylate and the remaining carboxylate group is free. Acid-3 connects the La–O–La chains completing the two-dimensional structure (Fig. 1c). The free C–OH group of acid-1 participates in intra-layer hydrogen bonding with bonded C–O group of the carboxylate of acid-2 (see ESI‡). The two-dimensional layers also exhibits hydrogen bond interactions involving the lattice water, [O(100)], coordinated water, [O(7)], free C–OH group of the carboxyalate of acid-2 and C–O group of carboxylate of acid-1 and acid-4 forming a three-dimensionally extended hydrogen bonded structure (see ESI‡). The complete list of the observed hydrogen bond interactions in **I** is given in Table 4.

The compounds **II** and **IIa** are isostructural and isomorphous and have 41 non-hydrogen atoms in the asymmetric unit, of which two M^{3+} (M = Y, Gd) are crystallographically independent. The isophthalate anions can be classified into three different types based on their coordination modes (see ESI‡). For describing the structure, we consider only the Y compound. Unlike **I**, the Y^{3+} ions show differences in their coordination with respect to the oxygens. Thus, Y(1) is seven coordinated with 5 carboxylate oxygens and

Table 4 Important hydrogen bond interactions in $[La_2(H_2O)][\{C_6H_4(COO)_2\}_2\{C_6H_4(COOH)(COO)\}_2]\cdot H_2O$, **I**

D–H···A	D–H/Å	H···A/Å	D···A/Å	D–H···A/°
O(22)–H(22)···O(1)[a]	0.82	1.96	2.750(3)	162
O(31)–H(31)···O(12)[b]	0.82	2.08	2.876(7)	164
O(7)–H(51)···O(100)	0.85	1.87	2.710(5)	170
O(7)–H(52)···O(32)[c]	0.85	2.15	2.992(4)	175
O(100)–H(101)···O(32)[d]	0.84	2.16	2.972(5)	164
O(100)–H(102)···O(11)[e]	0.84	2.11	2.923(5)	161

[a] x, $1/2 - y$, $-1/2 + z$. [b] $-1 + x$, $1 + y$, z. [c] $1 + x$, y, z. [d] $-x$, $-1/2 + y$, $1/2 - z$. [e] $1 - x$, $-1/2 + y$, $1/2 - z$.

2 water molecules and Y(2) is 8 coordinated with carboxylate oxygens, forming a mono-(CN = 7) and a bi-(CN = 8) capped trigonal prismatic arrangement (see ESI‡). Of the 15 oxygens, only one oxygen, O(6), has μ_3 connectivity linking two Y centers and a carbon, which forms a simple Y–O–Y dimeric unit. The Y–O bonds have distances in the range 2.228(3)–2.640(3) Å and O–Y–O bond angles are in the range 51.41(10)–157.66(13)°. Again, the coordination geometry around the central Y^{3+} ion is based on typical bond distances in the range 2.2–2.7 Å. Similar bond distances and angles have been observed before.[7e] Selected bond distances for compounds **II** and **IIa** are listed in Table 5.

The structure of **II** consists of $Y(1)O_5(H_2O)_2$ and $Y(2)O_8$ polyhedral units connected through a common oxygen vertex, O(6), forming a dimeric unit. In addition, the two Y^{3+} ions are also connected by carboxylate units forming the typical building unit commonly observed in many metal-organic framework compounds (Fig. 2a).[7f] The dimer units are connected by two different isophthalate anions (acid-1 and acid-3) to give rise to a one-dimensional chain-like structure. As can be noted, the chains lie on the 2_1 axis giving rise to a helical nature (Fig. 2b). The chains are connected through the acid-2 completing the two-dimensional layer structure (Fig. 2c). The coordinated water, O(3), participate in strong intra-layer hydrogen bonding with the C–O group of the carboxylate of acid-2, which partially stabilizes the layers. In addition, the two-dimensional layers are connected with each other through hydrogen bond interaction involving the coordinated water, ([O(7)], lattice water, [O(100)] and C–O group of the carboxylate of acid-1 (see ESI‡). The complete list of the observed hydrogen bond interactions is given in Table 6.

Table 5 Selected bond distances (Å) observed in $[M_2(H_2O)_2][\{C_6H_4(COO)_2\}_3]\cdot H_2O$, M = Y(**II**), Gd(**IIa**)

Bonds	Y(**II**)	Gd(**IIa**)
M(1)–O(1)	2.277(3)	2.318(3)
M(1)–O(2)	2.228(3)	2.267(3)
M(1)–O(3)	2.363(4)	2.423(3)
M(1)–O(4)	2.350(3)	2.417(3)
M(1)–O(5)	2.258(3)	2.316(3)
M(1)–O(6)	2.366(3)	2.396(3)
M(1)–O(7)	2.297(4)	2.345(3)
M(2)–O(6)	2.640(3)	2.640(3)
M(2)–O(8)	2.269(3)	2.322(3)
M(2)–O(9)	2.276(3)	2.342(3)
M(2)–O(10)[a]	2.271(3)	2.319(3)
M(2)–O(11)	2.392(3)	2.441(3)
M(2)–O(12)	2.495(3)	2.543(3)
M(2)–O(13)	2.418(3)	2.447(3)
M(2)–O(14)[a]	2.332(3)	2.369(3)

[a] Symmetry transformations used to generate equivalent atoms: $-x$, $y + 1/2$, $-z + 1/2$.

The role of $\pi\cdots\pi$/CH$\cdots\pi$ interactions in the stability of supramolecularly engineered crystal structures has been well documented.[13] In recent years, the role of $\pi\cdots\pi$/CH$\cdots\pi$ interactions in extended metal–organic frameworks have attracted much attention. This generally non-covalent interaction lends some stability to the low-dimensional structures. In the present compounds, we find significant intra-layer $\pi\cdots\pi$/CH$\cdots\pi$ interactions between the aromatic rings of the isophthalate anions. The distances between the aromatic rings and the inter-planar angle suggests that this type of interactions may be present in the following pair: In **I**, between two acid-1 and between acid-2 and acid-3 and in **II**, between acid-1 and acid-3 and between acid-2 and acid-3. To understand the nature and the energies involved in these interactions, we performed calculations using Gaussian98 software package at B3LYP/6-31+G(d,p) level.[14] Using the crystal structure geometry, the calculated energies for the interaction between the benzene rings were 1.24 kcal mol^{-1} (between two acid-1 in **I**), 1.29 kcal mol^{-1} (between acid-2 and acid-3 in **I**), 1.73 kcal mol^{-1} (between acid-1 and acid-3 in **II**) and 2.46 kcal mol^{-1} (between acid-2 and acid-3 in **II**). Thus, the net energy involved in these interactions appear to be too low to be of any significance.

It is illustrative to compare the structures exhibited by La^{3+} and Y^{3+} ions (**I** and **II**). As expected, the larger La^{3+} ions have 9 coordination compared to the 7 and 8 coordination for Y^{3+} ions. While the structure of **I** has four isophthalate anions, **II** has only three such units and both the structures have two M^{3+} ions. Both the structures are also formed with the same space group, $P2_1/c$ (no. 14). While the *a* and *b* parameters are comparable in both the structures, the *c* parameter in **I** is larger by ~4.4 Å. The larger size of the *c* lattice parameter can be explained by examining the structure of **I** and **II** in the *ac* plane (Fig. 3a and 3b). In **I**, the layers are formed in the *bc* plane and are stacked one over other in the *a* direction, whereas in **II**, the layers are formed in the *ab* plane and are stacked in the *c* direction. This difference in the arrangement of the layers is responsible for the observed differences in the *c* lattice parameter between **I** and **II**.

Luminescence studies. It has been shown that the lanthanide ions are useful as luminescent probes and the lanthanide centered emission can be sensitized by molecules having the π electrons.[1b] The low molar absorptivity of the lanthanides does not favor a strong emission when excited directly. Significant emission, characteristic of the lanthanide ions, however, can be observed by employing suitable complexing/chelating agents that can absorb and transfer the energy to the central lanthanide ions. Generally, in coordination complexes, the ligand is excited to the singlet state, from where part of the energy is transferred to the triplet state through inter system crossing. When the energy levels are favorable, the triplet excited state can transfer the energy to the

Table 6 Important hydrogen bond interactions in $[Y_2(H_2O)_2][\{C_6H_4(COO)_2\}_3]\cdot H_2O$, **II**

D–H$\cdots$A	D–H/Å	H$\cdots$A/Å	D$\cdots$A/Å	D–H$\cdots$A/°
O(3)–H(52)$\cdots$O(13)[a]	0.85	1.85	2.699(6)	178
O(7)–H(62)$\cdots$O(14)[b]	0.85	1.93	2.761(5)	165
O(7)–H(61)$\cdots$O(100)	0.84	1.85	2.690(5)	170

[a] $-x, -1/2 + y, 1/2 - z$. [b] $x, 1/2 - y, -1/2 + z$.

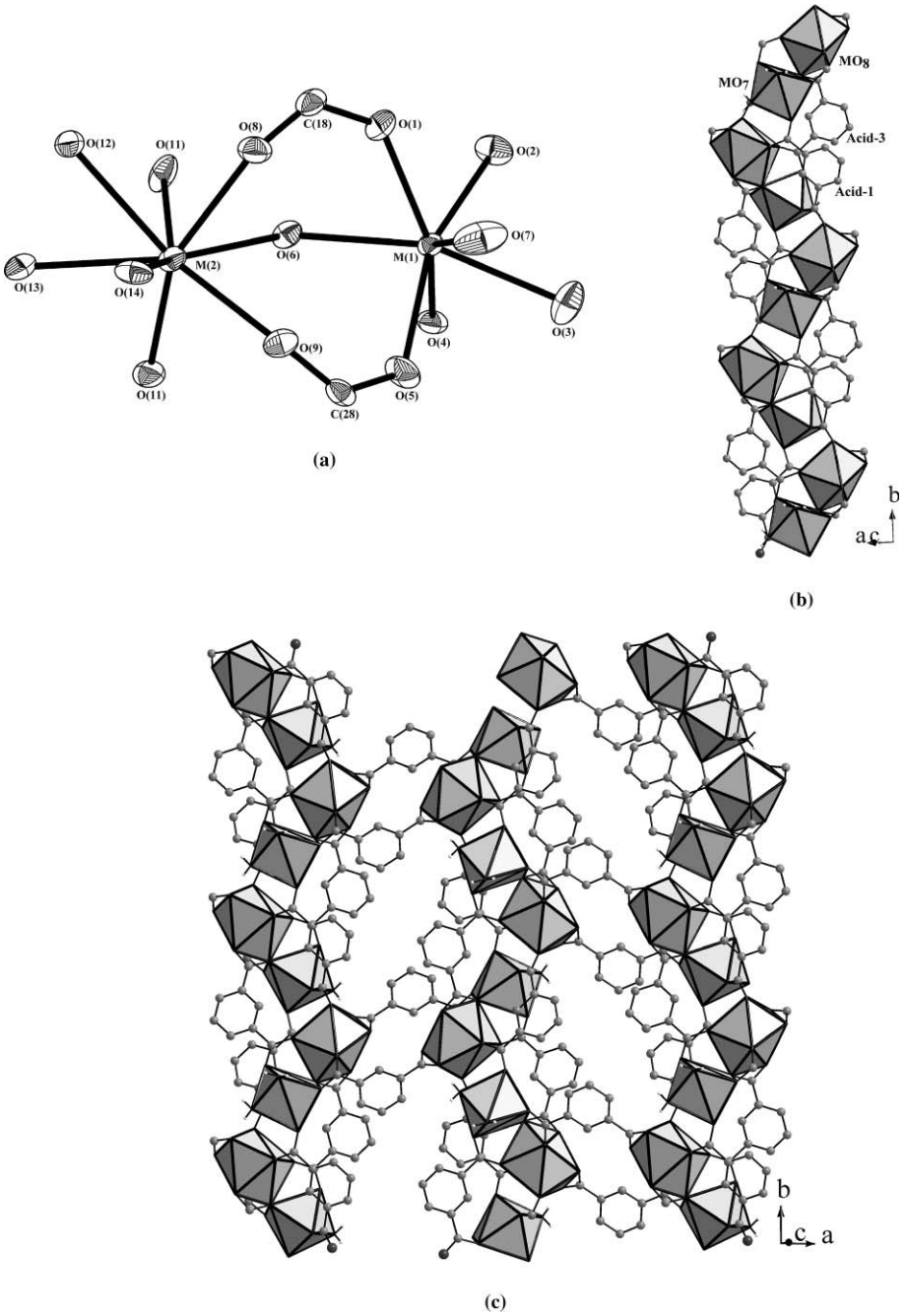

Fig. 2 (a) ORTEP[22] diagram showing the connectivity between $M(1)O_7$ and $M(2)O_8$ polyhedra through the μ_3 oxygen atoms in **II**. Thermal ellipsoids are given at 50% probability. Note the formation of a simple dimeric unit. (b) View of the one-dimensional chain formed by the connectivity between the dimeric unit and isophthalate anions (acid-1 and acid-2) in **II**. Note that the chains lie on the 2_1 axis. (c) View of the layer formed by the connectivity between the chains and acid-2 in **II**.

metal centers, resulting in metal centered luminescence.[15] The success of this transfer of energy is reflected in the suppressing of the intra-ligand emission in the luminescence spectra. In the present compounds, the isophthalate anions absorb strongly in the UV region and can sensitize the lanthanide ion.

The solid state photoluminescence spectra of compounds **I**, **Ic–If** and **II**, **IIc–IIf** were recorded at room temperature (Fig. 4a and b and Fig. 5a and b). The photoluminescence spectra of the sodium salt of the isophthalate, recorded at room temperature, showed a broad emission centered at 370 nm (λ_{ex} = 300 nm), which may be due to the $\pi^* \rightarrow n$ or $\pi^* \rightarrow \pi$ transition (see ESI‡). The parent compounds, **I** and **II** also exhibited a broad emission at 370 nm (λ_{ex} = 300 nm) along with low intense broad peaks in the range 415–500 nm, which could be due to other intra-ligand transitions.[16] The doped samples (Eu^{3+}, Tb^{3+}) in place of La and Y, on the other hand, exhibited a suppression of the intra-ligand band along with the observation of strong luminescence corresponding to the doped element (red = Eu^{3+}, green = Tb^{3+}) (Fig. 6). This

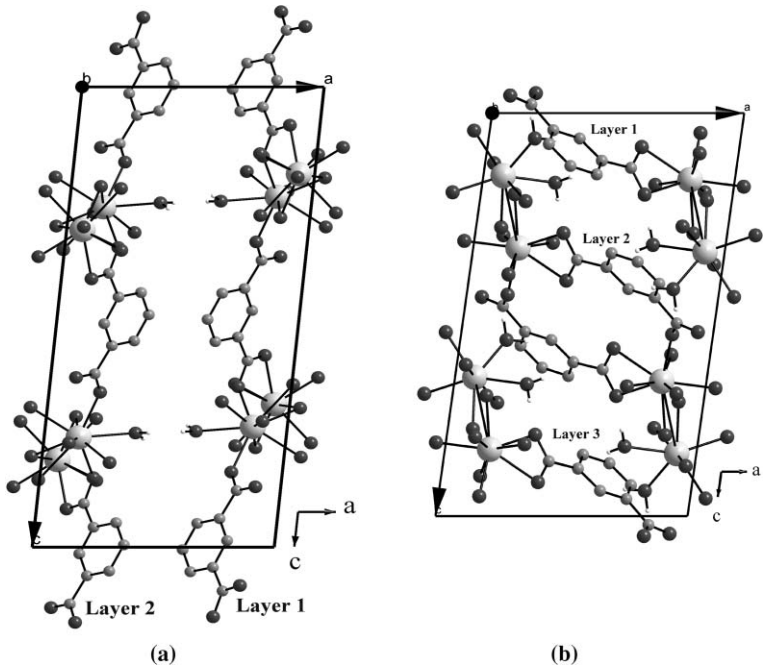

Fig. 3 (a) View of the layers in **I** in the *ac* plane. (b) View of the layers in **II** in the *ac* plane. Note the different arrangements (see text).

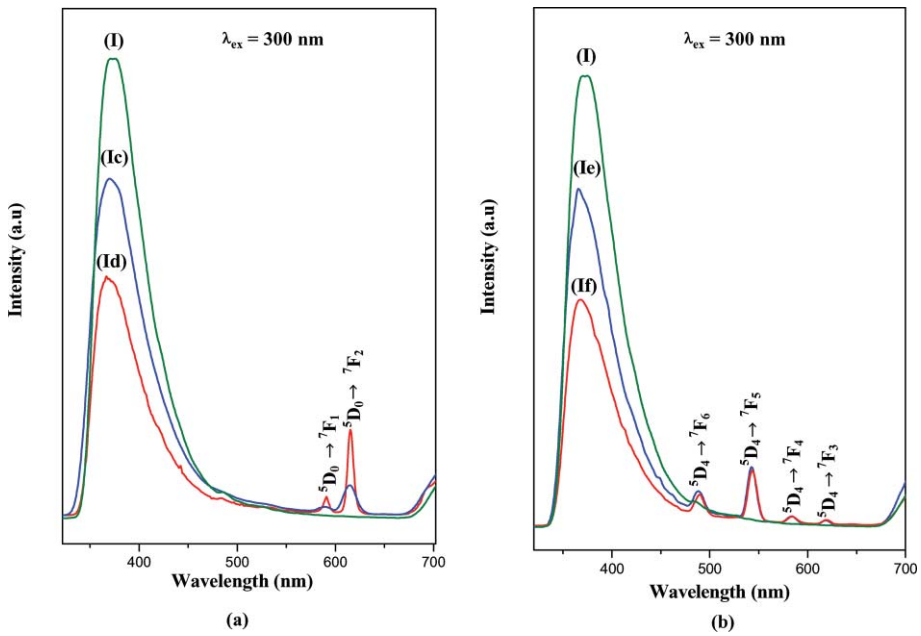

Fig. 4 (a) Room-temperature photoluminescence spectra of **I** and the corresponding Eu doped compounds, **Ic** (2 mol% Eu) and **Id** (4 mol% Eu). (b) Room-temperature photoluminescence spectra of **I** and the corresponding Tb doped compounds, **Ie** (2 mol% Tb) and **If** (4 mol% Tb). Note that in both the cases the intra-ligand transitions are suppressed on doping.

indicates that there is a successful and efficient energy transfer from the isophthalate anions to the metal centers.

As can be noted from Fig. 4a (Eu^{3+} doped in **I**) and Fig. 4b (Tb^{3+} doped in **I**), the main intra-ligand band is suppressed followed by the appearance of the characteristic $^5D_0 \rightarrow {}^7F_J$ ($J = 1, 2$) emission bands for Eu^{3+} and $^5D_4 \rightarrow {}^7F_J$ ($J = 3, 4, 5, 6$) emission bands for Tb^{3+}, when excited using $\lambda = 300$ nm. The emission bands at 590 and 614 nm (for **Ic** and **If**) corresponds to $^5D_0 \rightarrow {}^7F_1$ and $^5D_0 \rightarrow {}^7F_2$ transitions, respectively. Other possible $^5D_0 \rightarrow {}^7F_J$ transitions corresponding to $J = 0, 3, 4$ *etc*. are not visible in the present compounds, possibly, due to the low intensity. Compared to the 4% Eu-doped sample, the 2% Eu-doped sample shows larger intra-ligand emission indicating the higher dopant level facilitates the transfer of more energy from the isophthalate anions. This behavior may not be a linear one for higher concentrations of Eu^{3+} as the metal centered emission would start to undergo self quenching.[1b] For the Tb^{3+} doped compounds, the emission bands at 490, 540, 580 and 620 nm can be assigned to the $^5D_4 \rightarrow {}^7F_6$,

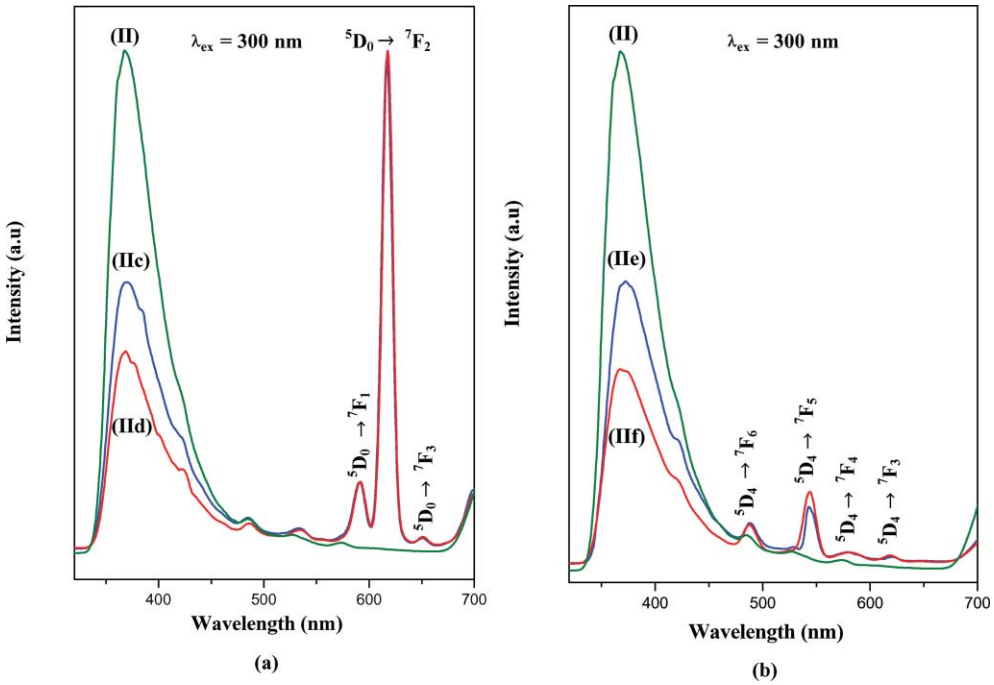

Fig. 5 (a) Room-temperature photoluminescence spectra of **II** and corresponding Eu doped compounds, **IIc** (2 mol% Eu) and **IId** (4 mol% Eu). (b) Room-temperature photoluminescence spectra of **II** and corresponding Tb doped compounds, **IIe** (2 mol% Tb) and **IIf** (4 mol% Tb). Note the suppression of the intra-ligand transitions.

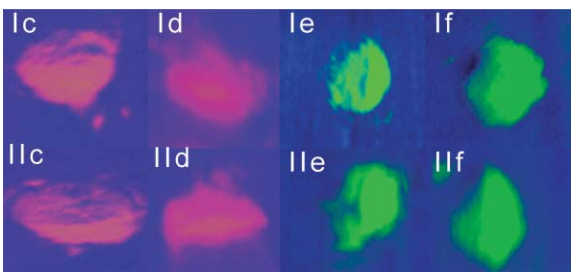

Fig. 6 View of the Eu- and Tb- doped samples under UV illumination.

$^5D_4 \rightarrow {}^7F_5$, $^5D_4 \rightarrow {}^7F_4$ and $^5D_4 \rightarrow {}^7F_3$ transitions, respectively. Again, the higher concentration of Tb^{3+} in **I** (**If**) shows more quenching of the intra-ligand transition, and also give rise to more intense green emission (Fig. 4b).

The Eu^{3+} doped (Fig. 5a) and Tb^{3+} doped (Fig. 5b) in place of Y (**II**) also show similar characteristic emission bands. The various observed band are: $^5D_0 \rightarrow {}^7F_1$ (~590 nm), $^5D_0 \rightarrow {}^7F_2$ (~616 nm) and $^5D_0 \rightarrow {}^7F_3$ (~650 nm) for the Eu^{3+} doped sample, and $^5D_4 \rightarrow {}^7F_6$ (~488 nm), $^5D_4 \rightarrow {}^7F_5$ (~542 nm), $^5D_4 \rightarrow {}^7F_4$ (~580 nm) and $^5D_4 \rightarrow {}^7F_3$ (~620 nm) for the Tb^{3+} doped samples.

A comparison of the photoluminescence studies of the doped samples in La (**I**) and Y (**II**) compounds indicate that the intra-ligand transition appears to be quenched more in the latter (Fig. 4 and 5). It is likely that the comparable size of Eu^{3+} and Tb^{3+} with Y^{3+} would have led to less local distortion, thereby, helping more efficient energy transfer [crystal radii for CN = 9 are 1.35 (La^{3+}), 1.26 (Eu^{3+}) and 1.24 (Tb^{3+}) Å; for CN = 8 are 1.159 (Y^{3+}), 1.21 (Eu^{3+}) and 1.18 (Tb^{3+}) Å, for CN = 7 are 1.10 (Y^{3+}), 1.15 (Eu^{3+}) and 1.12 (Tb^{3+}) Å].[17]

Up-conversion studies. Up-conversion is the excitation through a two stage process involving a reasonably stable intermediate. The up-conversion is really an anti-Stokes emission and may be used to detect infrared radiation visually. There has been considerable interest in studying new materials for the up-conversion process.[18] Most of the studies concentrate on cooperatively doped rare-earth ions in host lattices, pioneered by Auzel.[19] The use of lanthanide carboxylates for up-conversion studies has been attempted recently.[20] We, therefore, wanted to explore the up-conversion properties of the present compounds. Among the compounds, $[Nd_2(H_2O)][\{C_6H_4(COO)_2\}_2\text{-}\{C_6H_4(COOH)(COO)\}_2]\cdot H_2O$, **Ib**, appears to show promising up-conversion emissions. The UV-Vis spectra of **Ib** (Nd) is shown in Fig. 7a, which indicates that the absorption increases rapidly with decreasing wavelength below 300 nm due to the intra-ligand absorption. The absorption bands of the Nd^{3+} ions show detailed Stark splitting of the eigenstates by the crystal field effect.[21] However, the details of the Stark components in each level could not be resolved from the absorption spectrum at room temperature, because the thermally excited upper Stark levels of the ground state gives rise to additional absorption peaks superimposed on the zero-temperature peaks, resulting in a complicated pattern. A schematic diagram of the energy transfer process in the up-conversion using Nd^{3+} ions is shown in Fig. 7b. The denoted absorption bands of Nd^{3+} in Fig. 7a are involved in the up-conversion excitation levels. They are far from the intra-ligand absorption bands except for the $^4D_{3/2}$, $^4D_{5/2}$ bands. Since the luminescence (Fig. 7c) of **Ib** (Nd) at short wavelength results from the $^4D_{3/2}$ levels, the excitation of either the $^4D_{3/2}$ or $^4D_{5/2}$ band is required, and direct excitation is limited by the intra-ligand absorption by short wavelength radiation. On the other hand, the up-conversion

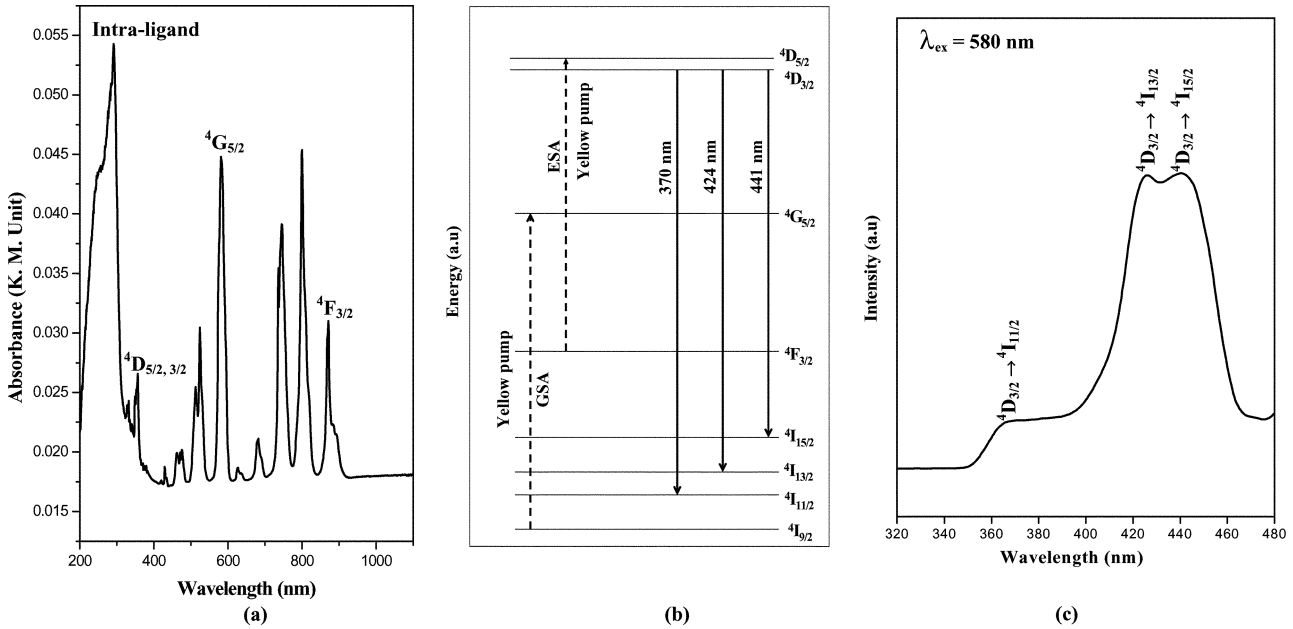

Fig. 7 (a) Absorption spectra of $[Nd_2(H_2O)][\{C_6H_4(COO)_2\}_2\{C_6H_4(COOH)(COO)\}_2]\cdot H_2O$, **Ib** at room temperature. (b) Schematic of the energy level diagram of Nd^{+3} ion in **Ib**. The dotted and solid arrow indicate yellow pumping (580 nm) and the transitions related to the luminescence, respectively. (c) Up-converted luminescence spectra of $[Nd_2(H_2O)][\{C_6H_4(COO)_2\}_2\{C_6H_4(COOH)(COO)\}_2]\cdot H_2O$, **Ib** at room temperature excited using 580 nm radiation.

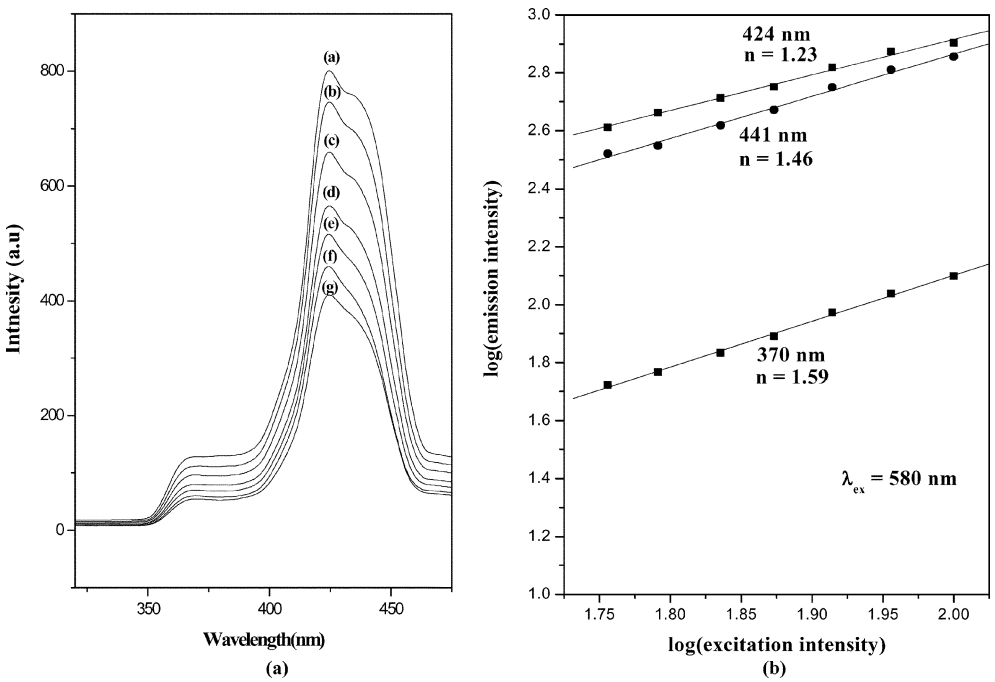

Fig. 8 (a) The observed emission dependence on the excitation intensity of $[Nd_2(H_2O)][\{C_6H_4(COO)_2\}_2\{C_6H_4(COOH)(COO)\}_2]\cdot H_2O$, **Ib**. (a) = 100%, (b) 90.31% (c) 82.07%, (d) 74.67%, (e) 68.5%, (f) 61.84% and (g) 57%. (b) The log–log plot of the excitation intensity dependence of the luminescence intensity at three different up-converted emission wavelengths (366, 424, and 441 nm).

excitation does not give rise to such problems because the excitation wavelength (≈ 580 nm) is far from the wavelength responsible for the intra-ligand absorption. The excitation wavelength (≈ 580 nm) was tuned to optimize the up-conversion excitation efficiency, of populating the $^4F_{3/2}$ levels and efficient re-excitation from the $^4F_{3/2}$ to the $^4D_{5/2}$ levels. The possible up-conversion excitation pathway (dashed line) and corresponding transitions (solid line) for the luminescence of Nd^{3+} ions are summarized in Fig. 7b. The excited $^4G_{5/2}$ levels relax nonradiatively to the $^4F_{3/2}$ levels where some populations take part in the excited state absorption (ESA) and the others relax to lower energy levels. The excited $^4D_{5/2}$ levels from the ESA also relax

nonradiatively to the $^4D_{3/2}$ levels from which up-converted luminescence is emitted. Fig. 7c shows the up-converted luminescence spectra from $^4D_{3/2}$ levels for 580 nm excitation (yellow pump). In order to understand the excitation intensity dependence of the up-converted luminescence intensity, we have carried out a simple experiment. In this, a series of sterile glass plates were placed sequentially in the pathway between the excitation source and the sample. The decrease in excitation intensity per glass plate has been determined from the UV-Vis spectroscopy. The successive decrease in the luminescence intensity using 6 different glass plates is shown in Fig. 8a. To find the number of photons involved in the up-conversion process, the luminescence intensity *versus* excitation intensity was plotted on a log–log scale (Fig. 8b). The three main regions (370, 424 and 441 nm) show a slope of greater than 1, indicating that in all cases the observed emission is a two-photon process. Similar values for the slopes have been obtained before for the two photon up-conversion processes in Nd^{3+} compounds.[19] The ideal value for the slope should be closer to 2 for the two photon absorption process, and the decreased value of the slope is, probably, due to the loss of the excitation energy at the one-photon absorption level, which might emit from $^4F_{3/2}$ to the $^4I_{11/2}$, $^4I_{9/2}$ level in the near-IR region. Further study is required to evaluate and understand the up-conversion process in these compounds.

Conclusions

Two different, but related, two-dimensional lanthanide benzene dicarboxylates have been prepared by hydrothermal methods. The structures consist of M^{3+} cations (M = lanthanides) and 1,3-benzenedicarboxylate anions connected to form the layered structure. Doping at the La^{3+} and Y^{3+} sites by Eu^{3+} and Tb^{3+} (2% and 4%) show red and green emission with characteristic transitions resulting from the ligand-sensitized energy transfer (or fluorescence resonance energy transfer). The Nd^{3+} containing compound exhibits up-conversion properties with intense blue emission when excited using 580 nm radiation.

Acknowledgements

SN thanks the Department of Science and Technology (DST), Government of India, for the award of a research grant and the authors thanks the Council of Scientific and Industrial Research (CSIR), Government of India, for the award of a fellowship (PM) and a research grant. DST-IRHPA is thanked for the CCD facility. SN also thanks the Department of Science and Technology (DST), Government of India, for the award of the RAMANNA fellowship.

References

1 (*a*) J. C. G. Bunzli and G. R. Choppin, *Lanthanide Probes in life, Chemical and Earth Science, Theory and Practice*, Elsevier, Amsterdam, 1989; (*b*) G. Blasse and B. C. Grabmaier, *Luminescent Materials*, Springer, Berlin, 1994.
2 (*a*) A. Patra, C. S. Friend, R. Kapoor and P. N. Prasad, *Chem. Mater.*, 2003, **15**, 3650; (*b*) X. Wang, X. Kong, G. Shan, Y. Yu, Y. Sun, L. Feng, K. Chao, S. Lu and Y. Li, *J. Phys. Chem. B*, 2004, **108**, 18408.
3 (*a*) J. Xu and K. N. Raymond, *Angew. Chem., Int. Ed.*, 2000, **39**, 2745; (*b*) Y. Bretonniere, M. Mazzanti, J. Pecaut and M. M. Olmstead, *J. Am. Chem. Soc.*, 2002, **124**, 9012; (*c*) C. M. Zaleski, E. C. Depperman, J. W. Kampf, M. L. Kirk and V. L. Pecoraro, *Angew. Chem., Int. Ed.*, 2004, **43**, 3912.
4 (*a*) Z. Wang, M. Strobele, K. L. Zhang, H. J. Meyer, X. Z. You and Z. Yu, *Inorg. Chem. Commun.*, 2002, **5**, 230; (*b*) Y. Wan, L. Zhang, L. Jin, S. Gao and S. Lu, *Inorg. Chem.*, 2003, **42**, 4985; (*c*) A. Thirumurugan and S. Natarajan, *J. Mater. Chem.*, 2005, **15**, 4588; (*d*) C. Serre, F. Millange, C. Thouvenot, N. Gardant, F. Pelle and G. Ferey, *J. Mater. Chem.*, 2004, **14**, 1540; (*e*) A. W. H. Lam, W. T. Wang, S. Gao, G. Wen and X. X. Zhang, *Eur. J. Inorg. Chem.*, 2003, **1**, 149.
5 (*a*) X. D. Guo, G. S. Zhu, Q. R. Fang, M. Xue, G. Tian, J. Y. Sun, X. T. Li and S. L. Qui, *Inorg. Chem.*, 2005, **44**, 3850; (*b*) B. Zhang, P. Cheng, X. Y. Chen, C. Cheng, W. Shi, D. Z. Liao, S. P. Yan and Z. H. Jiang, *J. Am. Chem. Soc.*, 2004, **126**, 3012.
6 (*a*) P. Mahata and S. Natarajan, *Inorg. Chem.*, 2007, **46**, 1250; (*b*) A. Thirumurugan and S. Natarajan, *Crystal Growth Des.*, 2006, **6**, 983; (*c*) A. Thirumuragan and S. Natarajan, *Dalton Trans.*, 2004, 2923; (*d*) A. Thirumurugan and S. Natarajan, *Eur. J. Inorg. Chem.*, 2004, 762.
7 (*a*) A. D. Bettencourt-Dias, *Inorg. Chem.*, 2005, **44**, 2734; (*b*) Y. H. Wan, L. P. Jin, S. Gao and S. Z. Lu, *Inorg. Chem.*, 2003, **42**, 4985; (*c*) X. J. Zheng, T. T. Zheng and L. P. Jin, *J. Mol. Struct.*, 2005, **740**, 31; (*d*) Y. H. Wan, L. P. Zhang and L. P. Jin, *J. Mol. Struct.*, 2003, **658**, 253.
8 K. Nakamoto, *Infrared and Raman Spectra of Inorganic and Coordination Compounds*, Wiley-Interscience Publication, New York, 1963.
9 *SMART (V 5.628), SAINT (V 6.45a), XPREP, SHELXTL*, Bruker AXS Inc., Madison, WI, 2004.
10 G. M. Sheldrick, *Siemens area correction absorption correction program*, University of Göttingen, Göttingen,Germany, 1994.
11 G. M. Sheldrick, *SHELXL-97 program for crystal structure solution and refinement*, University of Göttingen, Göttingen, Germany, 1997.
12 J. L. Farrugia, WinGx suite for small-molecule single crystal crystallography, *J. Appl. Crystallogr.*, 1999, **32**, 837.
13 (*a*) C. A. Hunter and J. K. M. Sander, *J. Am. Chem. Soc.*, 1990, **112**, 5525; (*b*) C. A. Hunter, J. Singh and J. K. M. Sander, *J. Mol. Biol.*, 1991, **218**, 837.
14 M. J. Frisch, G. W. Trucks, H. B. Schlegel, G. E. Scuseria, M. A. Robb, J. R. Cheeseman, V. G. Zakrzewski, J. A. Montgomery, Jr., R. E. Stratmann, J. C. Burant, S. Dapprich, J. M. Millam, A. D. Daniels, K. N. Kudin, M. C. Strain, O. Farkas, J. Tomasi, V. Barone, M. Cossi, R. Cammi, B. Mennucci, C. Pomelli, C. Adamo, S. Clifford, J. Ochterski, G. A. Petersson, P. Y. Ayala, Q. Cui, K. Morokuma, P. Salvador, J. J. Dannenberg, D. K. Malick, A. D. Rabuck, K. Raghavachari, J. B. Foresman, J. Cioslowski, J. V. Ortiz, A. G. Baboul, B. B. Stefanov, G. Liu, A. Liashenko, P. Piskorz, I. Komaromi, R. Gomperts, R. L. Martin, D. J. Fox, T. Keith, M. A. Al-Laham, C. Y. Peng, A. Nanayakkara, M. Challacombe, P. M. W. Gill, B. G. Johnson, W. Chen, M. W. Wong, J. L. Andres, C. Gonzalez, M. Head-Gordon, E. S. Replogle and J. A. Pople, *GAUSSIAN 98 (Revision A.11)*, Gaussian, Inc., Pittsburgh, PA, 2001.
15 (*a*) B. D. Chandler, D. T. Cramb and G. K. H. Shimizu, *J. Am. Chem. Soc.*, 2006, **128**, 10403; (*b*) P. R. Selvin, *Nat. Struct. Biol.*, 2000, **7**, 730; (*c*) R. E. Whan and G. A. Crosby, *J. Mol. Spectrosc.*, 1962, **8**, 315.
16 L. Wen, Y. Li, Z. Lu, J. Lin, C. Duan and Q. Men, *Crystal Growth Des.*, 2006, **6**, 530.
17 Y. Q. Jia, *J. Solid State Chem.*, 1991, **95**, 184.
18 (*a*) F. Auzel, *C. R. Acad. Sci. Paris*, 1966, 1016; (*b*) J. C. Wright, *Topics in Applied Physics: Radiationless Processes in Molecules and Condensed Phases*, ed. F. K. Fong, Springer, Berlin, 1976; (*c*) B. Layne, W. H. Lowdermilk and M. Weber, *J. Phys. Rev. B.*, 1997, **16**, 10.
19 F. Auzel, *Chem. Rev.*, 2004, **104**, 139.
20 J. Yang, Q. Yue, G. D. Li, J. J. Cao, G. H. Li and J. S. Chen, *Inorg. Chem.*, 2006, **45**, 2857.
21 J. J. Ju, T. Y. Kwon, H. K. Kim, J. H. Kim, S. C. Kim, M. Cha and S. I. Yun, *Mater. Lett.*, 1996, **29**, 13.
22 J. L. Farrugia, *J. Appl. Crystallogr.*, 1997, **30**, 565.

